Electronic Supplementary Material (ESI) for ChemComm.

Supporting Information

A Genuine Germylene PGeP Pincer Ligand for Formic Acid Dehydrogenation with Iridium

Marta Fernández-Buenestado,[†a] Rosie J. Somerville,[†a] Joaquín López-Serrano*[a], Jesús Campos*[a]

[a].Instituto de Investigaciones Químicas (IIQ), Departamento de Química Inorgánica and Centro de Innovación en Química Avanzada (ORFEO-CINQA), Consejo Superior de Investigaciones Científicas (CSIC) and Universidad de Sevilla. Avenida Américo Vespucio 49, 41092 Sevilla, Spain.

† These authors contributed equally

Table of Contents

1. General considerations

All preparations and manipulations were performed by using standard Schlenk and glovebox techniques, under an atmosphere of argon and of high purity nitrogen, respectively. All solvents were dried, stored over 4 Å molecular sieves, and degassed prior to use. Toluene (C_7H_8), THF (C_4H_8O), diethyl ether ($(CH_3CH_2)_2O$) and *n*-pentane (C_5H_{12}) were distilled under nitrogen over sodium. [D_8]-THF was dried over sodium and distilled under argon and CD_2Cl_2 was dried over CaH_2 and distilled under argon. $[IrCl(CO)(PPh_3)_2]$,[1] the precursors $(HN(CH_2)_3P^tBu_2)_2(o\text{-}C_6H_4)$[2a,b] and $Ge[N(SiMe_3)_2]_2$[3a,b] and the $NaBAr^F$ ($C_{32}H_{12}BF_{24}Na$)[4] salt were prepared as described previously. All other reagents were used as received from commercial suppliers. Solution NMR spectra were recorded with Bruker AVANCE NEO-300, AVANCE NEO-400, AVANCE III-400 and AVANCE NEO-500 spectrometers. Spectra were referenced to external $SiMe_4$ (δ: 0 ppm) by using the residual proton solvent peaks as internal standards (^{1}H NMR experiments), or the characteristic resonances of the solvent nuclei (^{13}C NMR experiments), while ^{31}P was referenced to H_3PO_4. The following abbreviations and their combinations are used: br, broad; s, singlet; d, doublet; t, triplet; m, multiplet. The ^{1}H and ^{13}C signals were assigned by means of 2D HSQC and HMBC experiments. Infrared spectra were recorded with a Bruker Vector 22 spectrometer and sampling preparation was made in Nujol inside the glovebox. For elemental analyses a LECO TruSpec CHN elementary analyser was utilized. NMR signals for $[BAr^F]^-$ anion: **^{1}H NMR** (400 MHz, C_6D_6, 25˚C) δ: 8.39 (s, 8 H, *o*-CH), 7.66 (s, 4 H, *p*-CH). **^{19}F{^{1}H} NMR** (376 MHz, C_6D_6, 25˚C) δ: -62.1 ppm (s, CF_3). **^{13}C{^{1}H} NMR** (100 MHz, C_6D_6, 25˚C) δ: 135.1 (br, *o*-CH), 129.0 (s, *m*-*C*CF_3), 126.0 (s, *ipso*-CB), 123.4 (s, CF_3), 117.8 (m, *p*-CH).

2. Synthesis and characterization of new compounds

$Ge(N(CH_2)_3P^tBu_2)_2(o\text{-}C_6H_4)$ (compound 2)

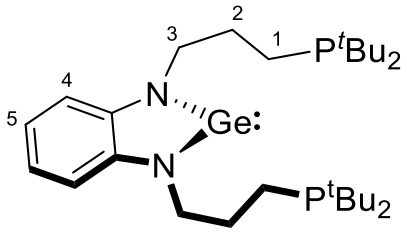

In a J. Young ampoule, a mixture of compounds $(HN(CH_2)_3P^tBu_2)_2(o\text{-}C_6H_4)$ (190 mg, 0.395 mmol) and $Ge[N(SiMe_3)_2]_2$ (158 mg, 0.402 mmol) was stirred in toluene (5.5 mL) at 55 ºC overnight. The solution was transferred to a vial and dried under vacuum in the glovebox until a dark orange oily residue was obtained. This was dissolved in as little pentane as possible and left in the freezer for a day. An orange solid-oily residue was obtained. The pentane was decanted with a pipette and the orange residue was dried under vacuum (197 mg, 90 %).

$^{31}P\{^1H\}$ NMR (160 MHz, C_6D_6, 25˚C) δ: 26.2 (s, P^tBu_2).

^1H NMR (400 MHz, C_6D_6, 25˚C) δ: 7.15 (s, 2 H, $CH^{(4)}$-C_6H_4), 7.14 (s, 2 H, $CH^{(5)}$-C_6H_4), 4.02 (t, 4 H, $^3J_{HH}$ = 7.2 Hz, $CH_2^{(3)}$) 2.15 (m, 4 H, $CH_2^{(2)}$), 1.39 (td, 4 H, $^3J_{HH}$ = 7.8 Hz, J_{HP} = 3.5 Hz, $CH_2^{(1)}$), 1.06 (d, 36 H, $^3J_{HP}$ = 10.7 Hz, ^{t}Bu).

$^{13}C\{^1H\}$ NMR (100 MHz, C_6D_6, 25˚C) δ: 143.0 (s, *ipso*-C_6H_4), 118.8 (s, $CH^{(5)}$-C_6H_4), 109.7 (s, $CH^{(4)}$-C_6H_4), 47.8 ($^3J_{CP}$ = 14 Hz, $CH_2^{(3)}$), 32.4 ($^2J_{CP}$ = 25 Hz, $CH_2^{(2)}$), 31.4 ($^1J_{CP}$ = 23 Hz, $C(CH_3)_3$), 29.8 ($^2J_{CP}$ = 14 Hz, $C(CH_3)_3$), 19.5 (d, $^1J_{CP}$ = 23 Hz, $CH_2^{(1)}$).

[Ir{κ^3*P,Ge,P*-GeCl(N(CH$_2$)$_3$P^{t}Bu$_2$)$_2$(*o*-C$_6$H$_4$)}CO] (compound 3)

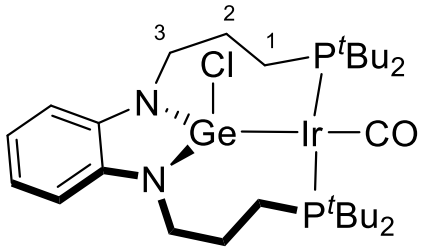

In a J. Young ampoule, a mixture of compounds **1** (102.4 mg, 0.19 mmol) and [IrCl(CO)(PPh$_3$)$_2$] (147.3 mg, 0.19 mmol) was stirred in THF (3 mL) and toluene (0.7 mL) at room temperature for one day. The mixture was filtered via cannula and the resulting orange solution was concentrated. Pentane was added (3 x 3 mL) to precipitate and wash the compound. The solid residue was left stirring in pentane (3 mL) for one day. The orange precipitate obtained was filtered off, washed again with pentane and dried in vacuo (84 mg, 55 %).

Anal. Calcd. for C$_{29}$H$_{52}$GeIrClN$_2$OP$_2$: C, 43.2; H,6.5; O, 2.0; N, 3.5. **Found**: C, 43.5; H, 6.1; N, 3.1.

^{31}P{^{1}H} NMR (160 MHz, C$_6$D$_6$, 25˚C) δ: 57.7 (br, Ir-P^{t}Bu$_2$).

^{31}P{^{1}H} NMR (160 MHz, THF-*d*$_8$, -15˚C) δ: 62.6 (d, $^2J_{PP}$ = 234 Hz, Ir-P^{t}Bu$_2$), 54.2 (d, $^2J_{PP}$ = 234 Hz, Ir-P^{t}Bu$_2$).

^{1}H NMR (400 MHz, C$_6$D$_6$, 25˚C) δ: 7.15 (m, 2 H, CH-C$_6$H$_4$), 6.91 (m, 2 H, CH-C$_6$H$_4$), 3.53 (br, 2 H, CH$_2^{(1)}$), 3.38 (br, 2 H, CH$_2^{(1)}$), 2.81 (br, 4 H, CH$_2^{(2)}$), 2.18 (br, 1 H, CH$_2^{(3)}$), 1.93 (br, 3 H, CH$_2^{(3)}$), 1.21 (d, 36 H, $^3J_{HP}$ = 45.4 Hz, ^{t}Bu).

^{13}C{^{1}H} NMR (100 MHz, C$_6$D$_6$, 25˚C) δ: 181.9 (s, Ir-CO), 117.4 (CH), 108.3 (CH), 46.5 (CH$_2^{(1)}$), 37.7 (*C*(CH$_3$)$_3$), 30.6 (s, C(*C*H$_3$)$_3$), 27.5 (s, CH$_2^{(2)}$), 25.9 (s, CH$_2^{(3)}$). The resonances due to some quaternary carbons could not be detected.

IR (Nujol): ν(Ir-CO) 1955 cm^{-1}.

[Ir{κ^3*P,Ge,P*-Ge(N(CH$_2$)$_3$P^{t}Bu$_2$)$_2$(*o*-C$_6$H$_4$)}(CO)]BAr^F (compound 4)

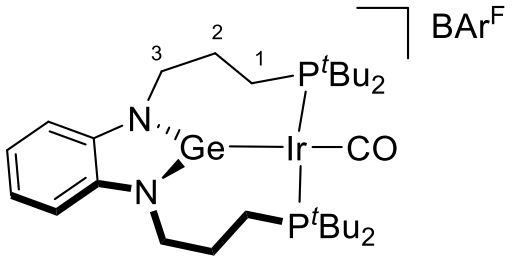

In a J. Young ampoule, compound **3** (82.5 mg, 0.102 mmol) was dissolved in diethyl ether (3 mL), the NaBAr^F salt was added (91 mg, 0.103 mmol) and the resulting solution was stirred at room temperature for one hour. The solution was filtered through one centimetre of celite, collected in a vial and allowed to evaporate slowly until the formation of red crystals (110 mg, 66 %).

Anal. Calcd. for $C_{61}H_{64}BF_{24}GeIrN_2OP_2$: C, 44.8; H, 4.0; O, 1; N, 1.7. **Found**: C, 44.7; H, 4.1; N, 1.7.

^{31}P{^{1}H} NMR (200 MHz, C_6D_6, 25˚C) δ: 64 (s, Ir-P^{t}Bu$_2$).

^{1}H NMR (500 MHz, C_6D_6, 25˚C) δ: 7.08 (m, 2 H, CH-C$_6$H$_4$), 6.80 (m, 2 H, CH-C$_6$H$_4$), 3.37 (m, 2 H, CH$_2^{(1)}$), 3.22 (m, 2 H, CH$_2^{(1)}$), 2.71 (br, 2 H, CH$_2^{(2)}$), 1.82 (br, 2 H, CH$_2^{(3)}$), 1.72 (br, 2 H, CH$_2^{(3)}$), 1.35 (d, $^3J_{HH}$ = 13.9 Hz, 2 H, CH$_2^{(2)}$), 0.97 (br, 18 H, ^{t}Bu), 0.79 (br, 18 H, ^{t}Bu).

^{13}C{^{1}H} NMR (125 MHz, C_6D_6, 25˚C) δ: 139.8 (*ipso*-C$_6$H$_4$), 121.6 (s, CH-C$_6$H$_4$), 110.0 (s, CH-C$_6$H$_4$), 47.6 (br, CH$_2^{(1)}$), 32.8 (s, *C*(CH$_3$)$_3$), 30.0 (s, C(*C*H$_3$)$_3$), 29.4 (s, C(*C*H$_3$)$_3$), 25.3 (s, CH$_2^{(2)}$), 23.1 (s, CH$_2^{(3)}$). The resonance of the carbonyl carbon could not be detected.

IR (Nujol): ν(Ir-CO) 1983 cm^{-1}.

[Ir{κ^3*P,Ge,P*-Ge(N(CH$_2$)$_3$P^{t}Bu$_2$)$_2$(*o*-C$_6$H$_4$)}(CO)(H)$_2$]BAr^F (compound 5)

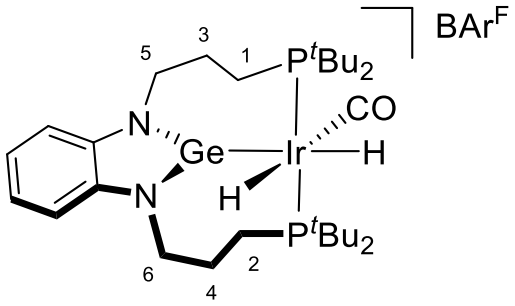

In a J. Young NMR tube, complex **3** and the NaBAr^F salt were mixed to obtain complex **4**. The solution was then frozen, the headspace evacuated, then the NMR tube filled with 1 bar of H_2, observing the disappearance of colour from the solution. Compound **5** was formed in 58% spectroscopic yield, though attempts to isolate it as a solid failed due to high instability and reversible dissociation of dihydrogen.

^{31}P{^{1}H} NMR (200 MHz, C_6D_6, 25˚C) δ: 67.6 (br, Ir-P^{t}Bu$_2$), 64.8 (br, Ir-^{t}Bu$_2$).

^{31}P{^{1}H} NMR (160 MHz, CD_2Cl_2, -40˚C) δ: 67.2 (d, $^2J_{PP}$ = 210 Hz, Ir-P^{t}Bu$_2$), 62.9 (d, $^2J_{PP}$ = 210 Hz, Ir-^{t}Bu$_2$).

^{1}H NMR (500 MHz, C_6D_6, 25˚C) δ: 7.06 (dd, 2 H, $^3J_{HH}$ = 5.8 Hz, $^3J_{HH}$ = 3.1 Hz, CH-C$_6$H$_4$), 6.76 (br, CH-C$_6$H$_4$), 3.34 (br, CH$_2$), 1.69 (br, CH$_2$), 0.83 (d, 18 H, $^3J_{HP}$ = 13.8 Hz, C(CH$_3$)$_3$), -11.94 (m, 1 H, Ir-H), -12.89 (m, 1 H, Ir-H).

^{1}H NMR (400 MHz, CD_2Cl_2, -40˚C) δ: 7.05 ppm (s, 4 H, CH-C$_6$H$_4$), 4.23 (m, 2 H, CH$_2^{(1,2)}$), 3.96 (m, 2 H, CH$_2^{(1,2)}$), 3.32 (m, 1 H, 1 CH of CH$_2^{(5,6)}$), 2.95 (m, 1 H, 1 CH of CH$_2^{(5,6)}$), 2.62 (m, 1 H, 1 CH of CH$_2^{(3,4)}$), 2.53 (m, 1 H, 1 CH of CH$_2^{(3,4)}$), 2.38 (br, 1 H, 1 CH of CH$_2^{(3,4)}$), 2.23 (m, 1 H, 1 CH of CH$_2^{(3,4)}$), 1.74 (m, 1 H, 1 CH of CH$_2^{(5,6)}$), 1.56 (d, 1 H, J = 12.9 Hz, 1 CH of CH$_2^{(5,6)}$), 1.29 (d, 36 H, *J* = 14.7 Hz, C(CH$_3$)$_3$), -11.50 (t, 1H, $^2J_{HP}$ = 14.7 Hz, Ir-H), -12.54 (m, 1 H, Ir-H).

^{13}C{^{1}H} NMR (125 MHz, C_6D_6, 25˚C) δ: 120.6 (s, CH-C$_6$H$_4$), 109.3 (s, CH-C$_6$H$_4$), 48.4 (CH$_2$), 29.0 (C(*C*H$_3$)$_3$).

^{13}C{^{1}H} NMR (100 MHz, CD_2Cl_2, -40˚C) δ: 120.4 (s, CH-C$_6$H$_4$), 120.0 (s, CH-C$_6$H$_4$), 109.3 (s, CH-C$_6$H$_4$), 109.1 (s, CH-C$_6$H$_4$), 49.1 (s, CH$_2^{(1,2)}$), 48.9 (CH$_2^{(1,2)}$), 36.4 (m, *C*(CH$_3$)$_3$), 30.0 (s, C(*C*H$_3$)$_3$), 27.2 (s, CH$_2^{(5,6)}$), 25.8 (s, CH$_2^{(3,4)}$), 24.6 (s, CH$_2^{(3.4)}$), 22.2 (s, CH$_2^{(5,6)}$). The resonance of the carbonyl carbon could not be detected.

IR (Nujol): ν(Ir-CO) 2019.7 cm^{-1}.

3. NMR spectra of compounds

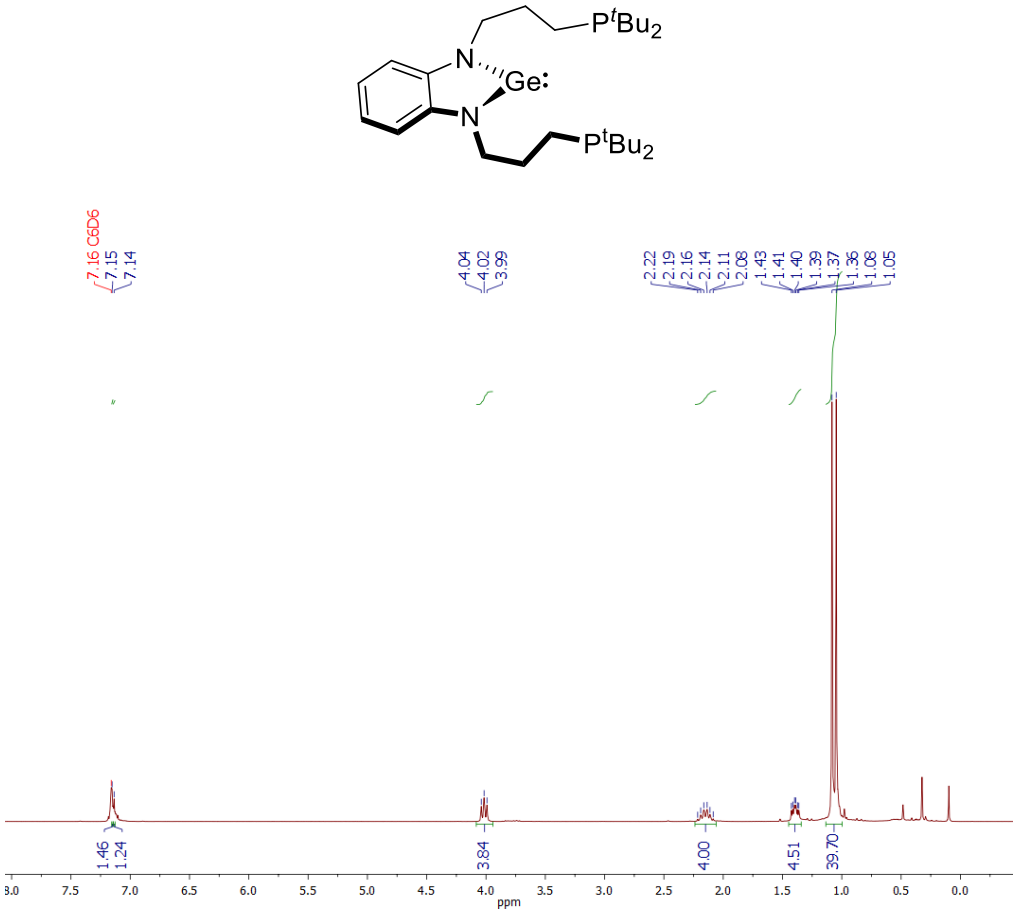

Figure S1. ^{1}H NMR (400 MHz, C_6D_6, 25 ºC) for compound **2**.

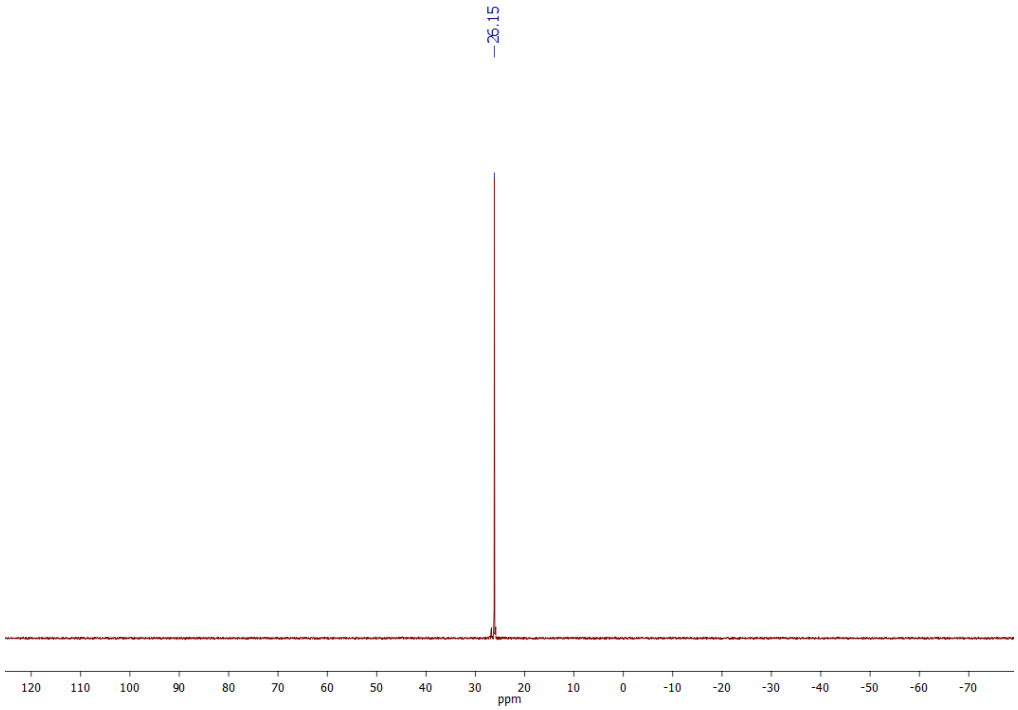

Figure S2. ^{31}P{^{1}H} NMR (160 MHz, C_6D_6, 25 ºC) for compound **2**.

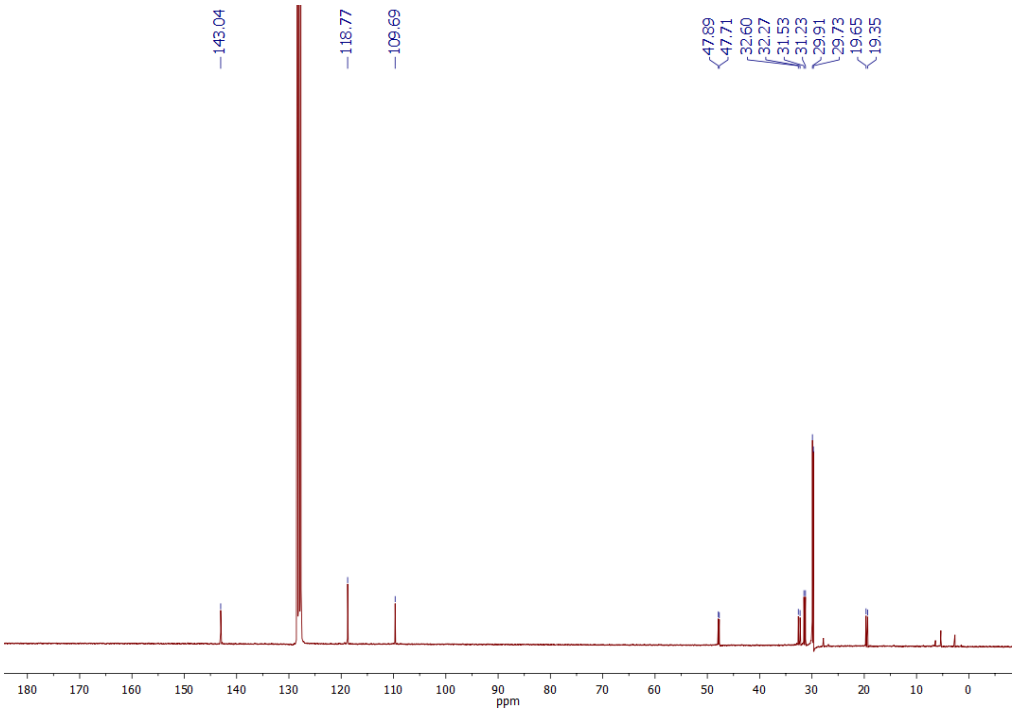

Figure S3. $^{13}C\{^{1}H\}$ NMR (100 MHz, C_6D_6, 25 ºC) for compound **2**.

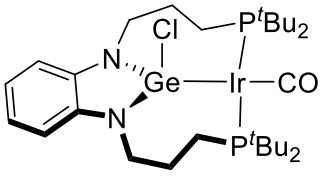

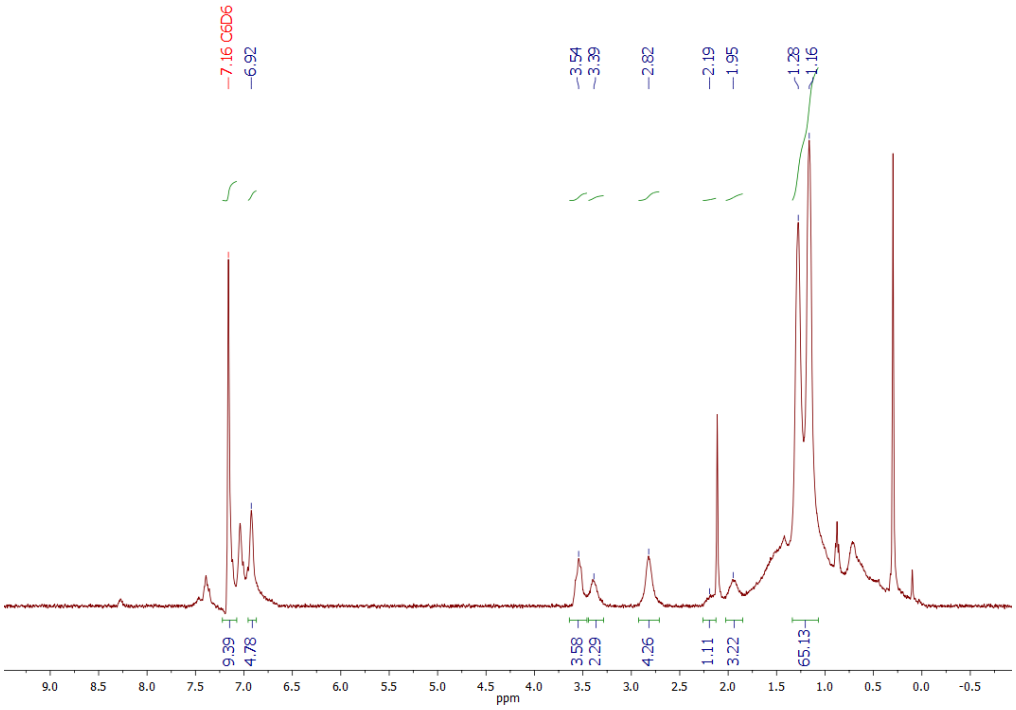

Figure S4. ^{1}H NMR (400 MHz, C_6D_6, 25 ºC) for compound **3**.

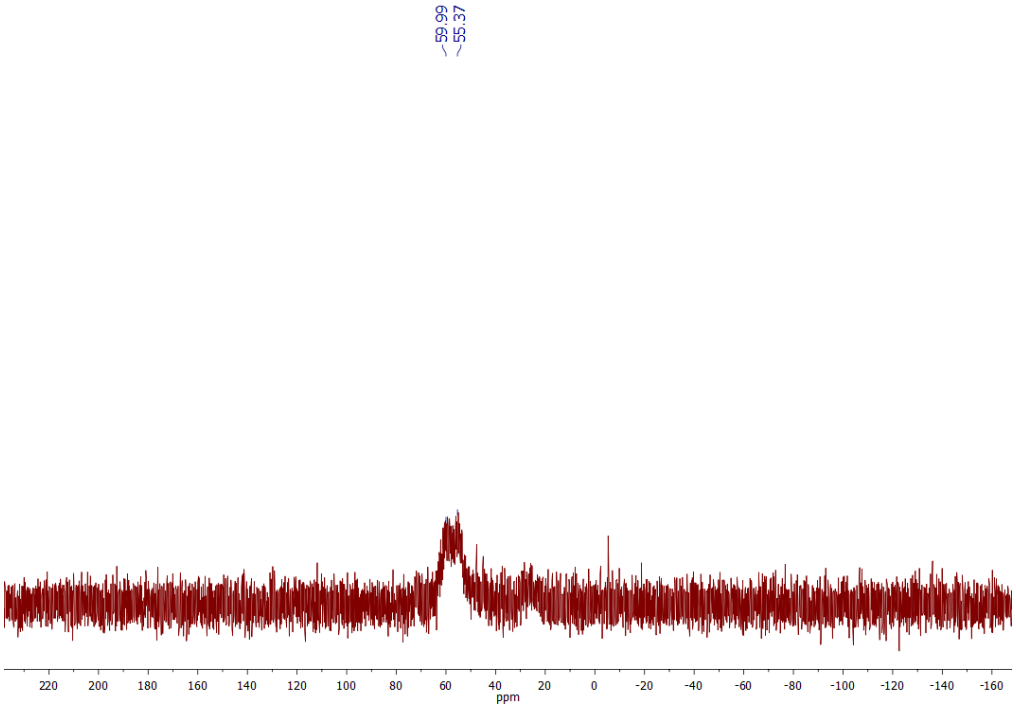

Figure S5. $^{31}P\{^{1}H\}$ NMR (160 MHz, C_6D_6, 25 ºC) for compound **3**.

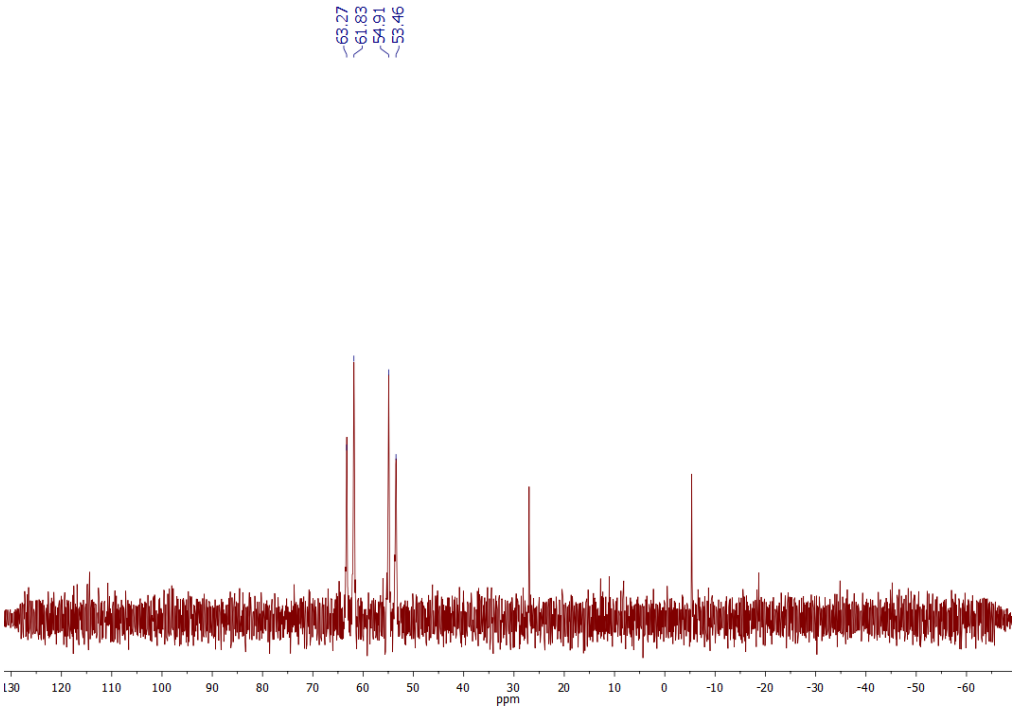

Figure S6. $^{31}P\{^{1}H\}$ NMR (160 MHz, THF-*d*8 -15 ºC) for compound **3** (minor signal at 26.2 ppm is due to PGeP ligand **2**; that at –6.0 ppm is due to PPh_3).

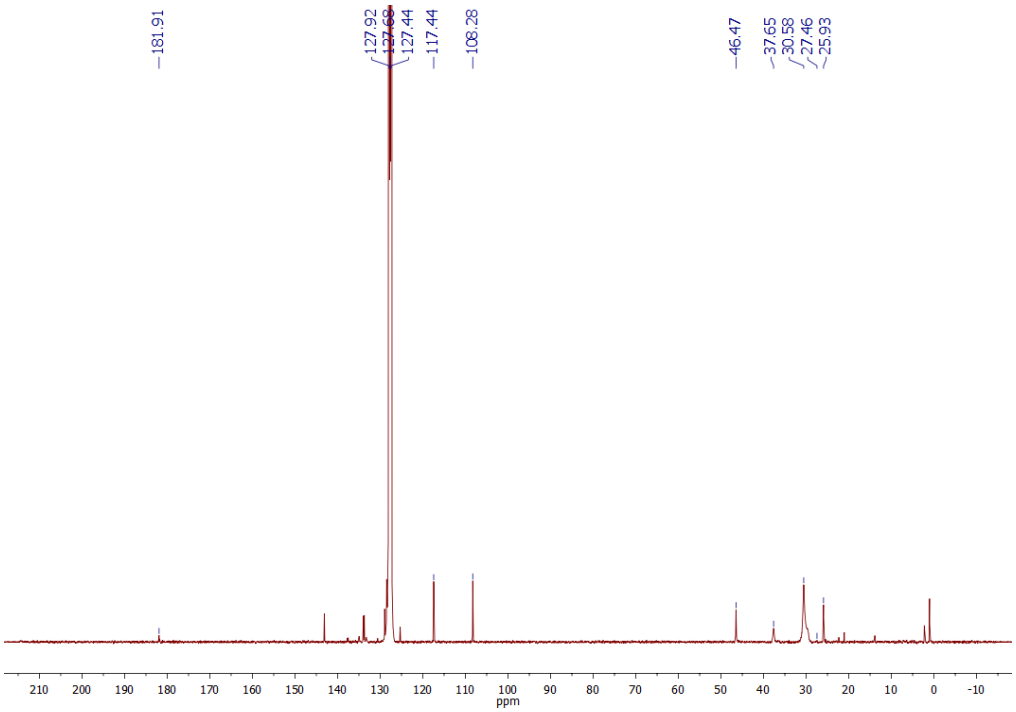

Figure S7. $^{13}C\{^{1}H\}$ NMR (100 MHz, C_6D_6, 25 ºC) for compound **3**.

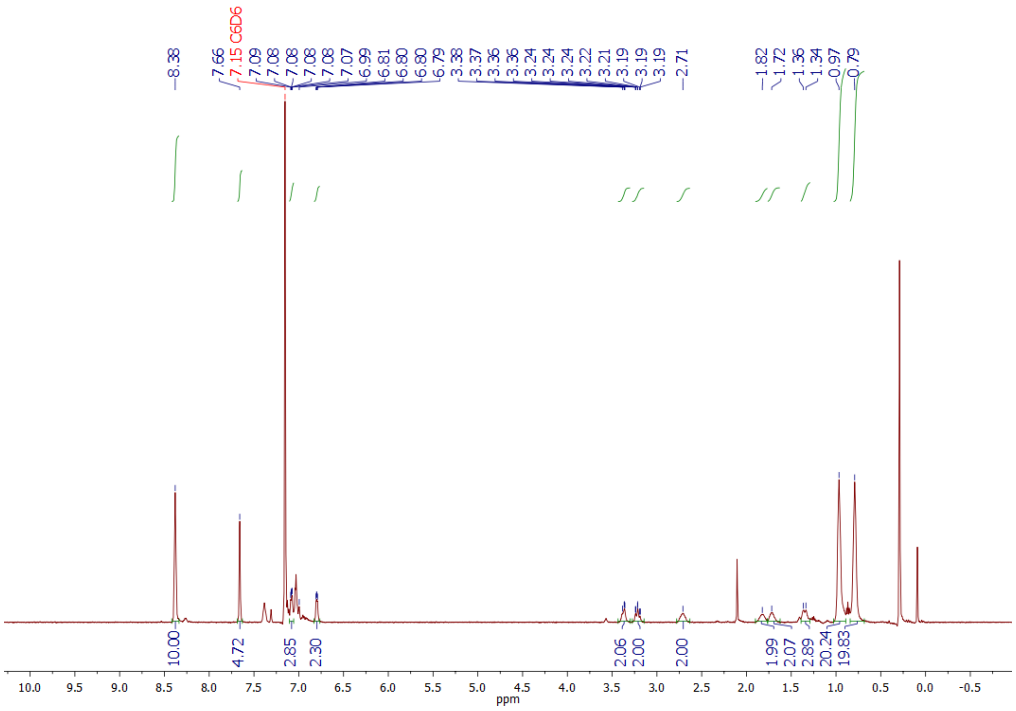

Figure S8. ^{1}H NMR (500 MHz, C_6D_6, 25 ºC) for compound **4**.

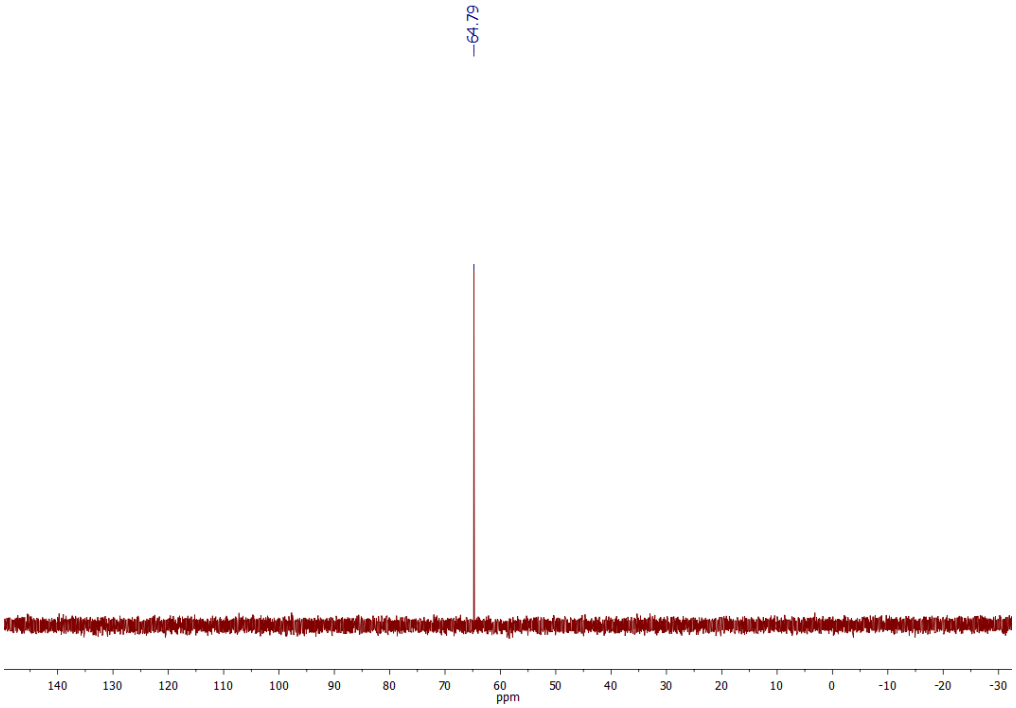

Figure S9. $^{31}P\{^{1}H\}$ NMR (200 MHz, C_6D_6, 25 ºC) for compound **4**.

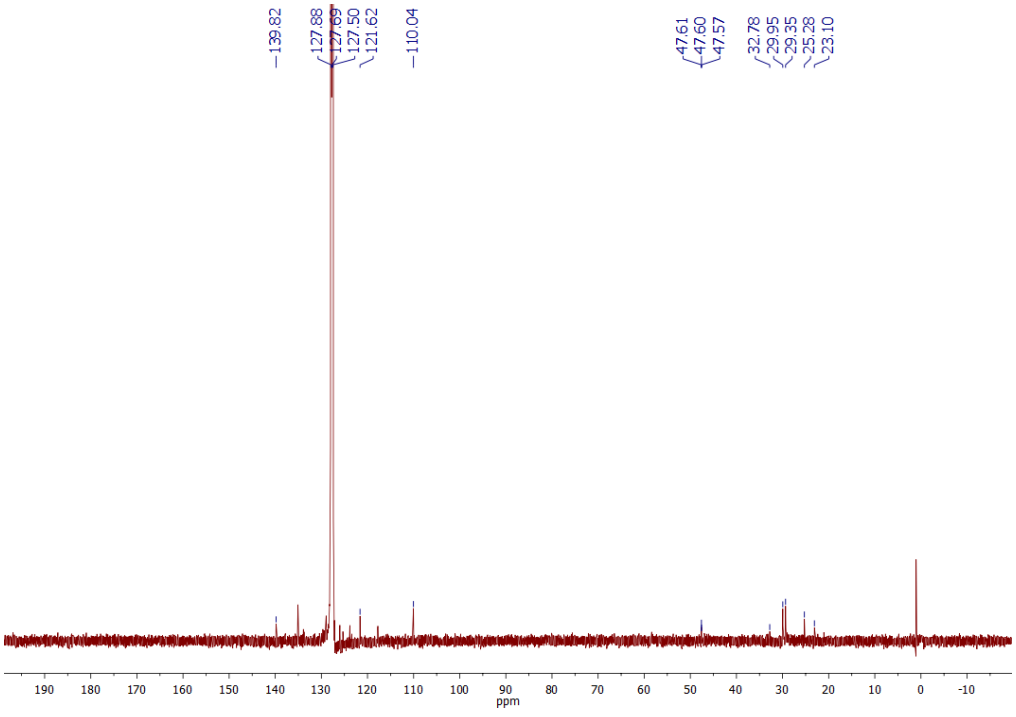

Figure S10. $^{13}C\{^{1}H\}$ NMR (125 MHz, C_6D_6, 25 ºC) for compound **4**.

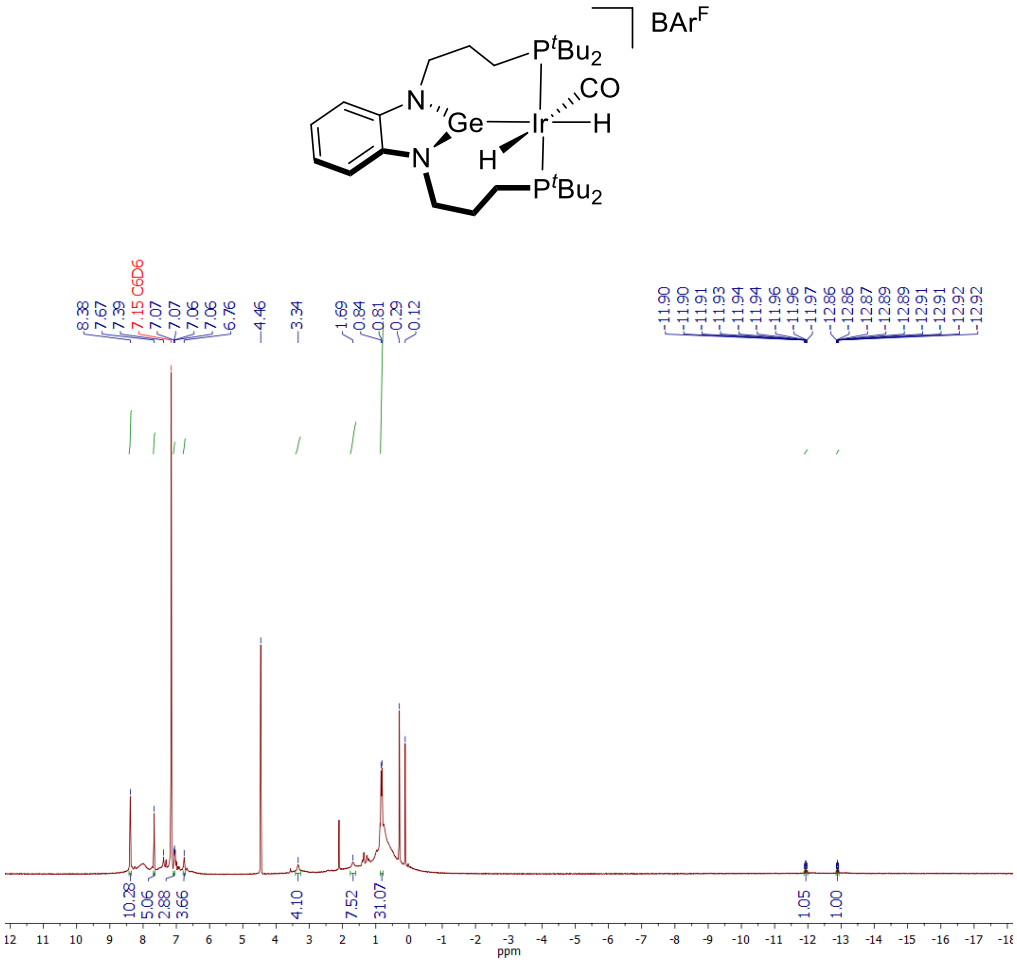

Figure S11. ^{1}H NMR (500 MHz, C_6D_6, 25 ºC) of the crude outcome of the reaction of compound **4** with H_2, showing the presence of compound **5**.

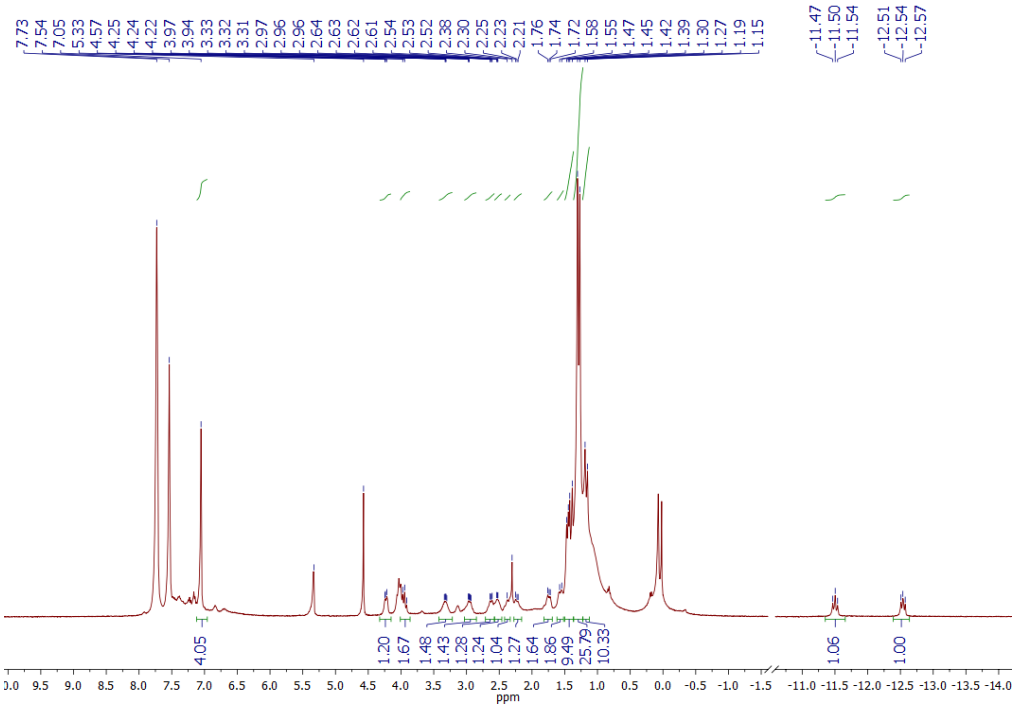

Figure S12. ^{1}H NMR (400 MHz, CD_2Cl_2, –40 ºC) of the crude outcome of the reaction of compound **4** with H_2, showing the presence of compound **5**.

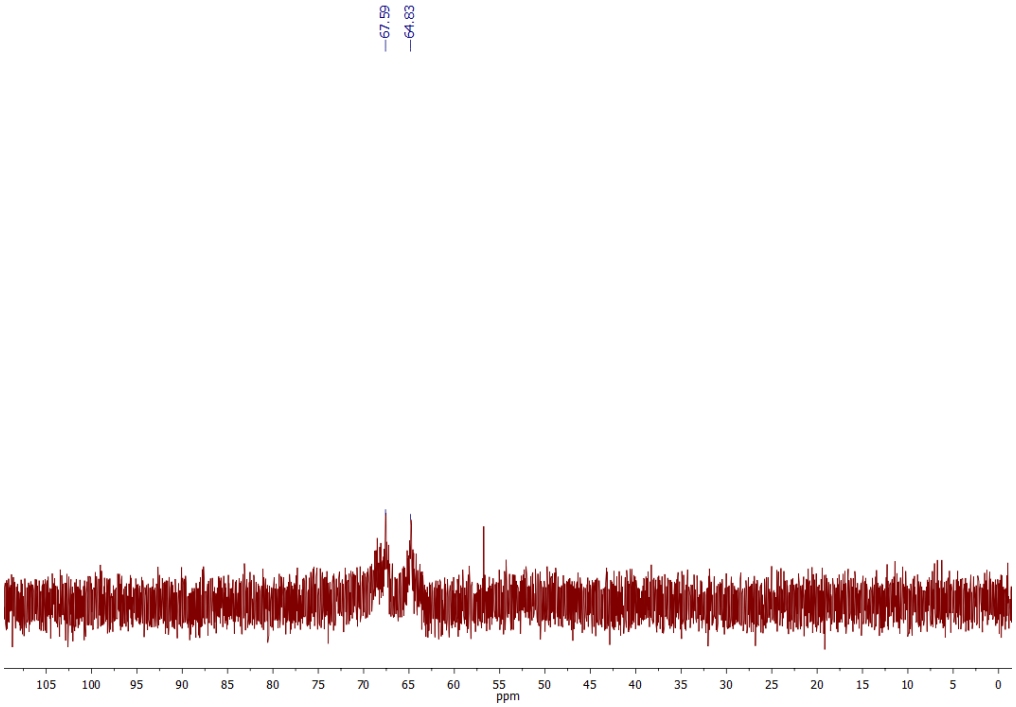

Figure S13. $^{31}P\{^{1}H\}$ NMR (200 MHz, C_6D_6, 25 ºC) of the crude outcome of the reaction of compound **4** with H_2, showing the presence of compound **5**.

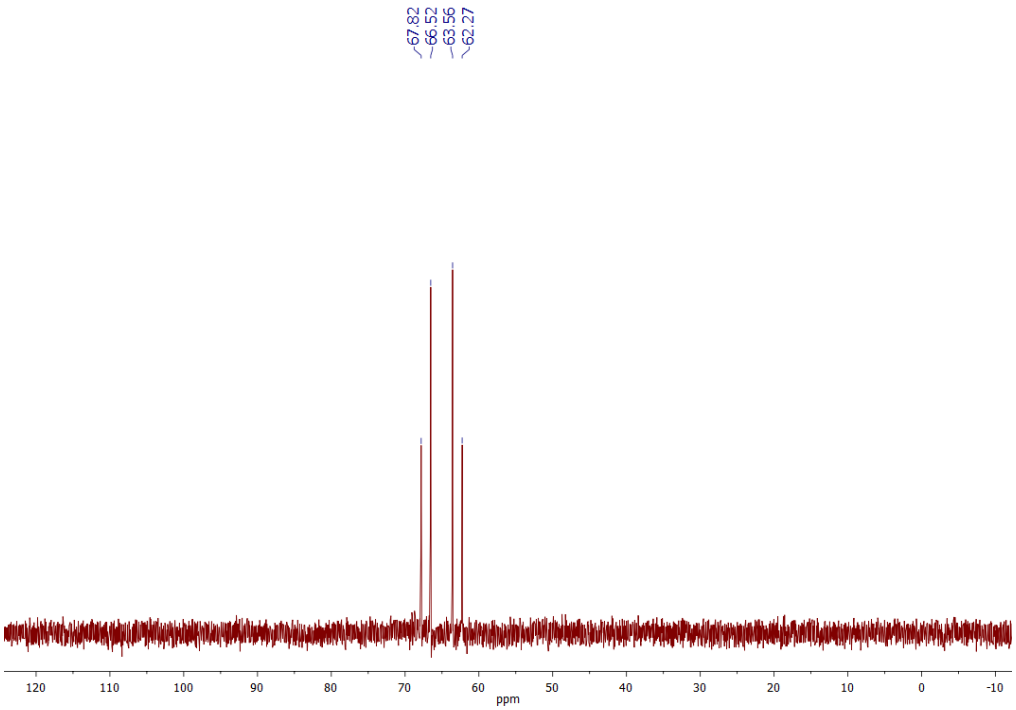

Figure S14. $^{31}P\{^{1}H\}$ NMR (160 MHz, CD_2Cl_2, –40 ºC) of the crude outcome of the reaction of compound **4** with H_2, showing the presence of compound **5**.

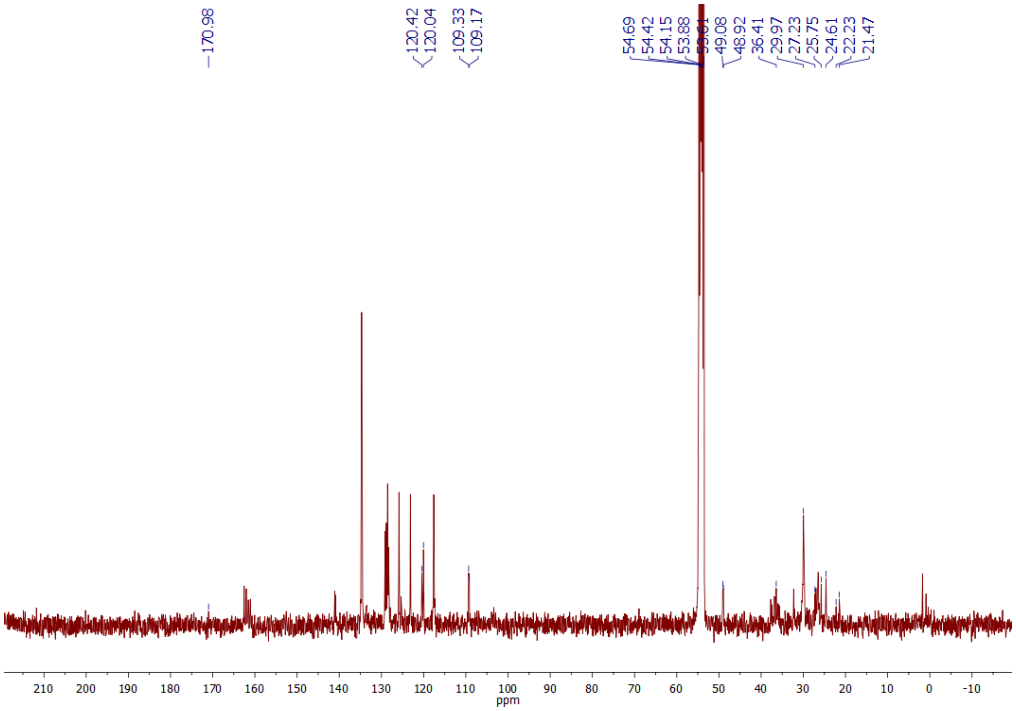

Figure S15. $^{13}C\{^{1}H\}$ NMR (100 MHz, CD_2Cl_2, –40 ºC) of the crude outcome of the reaction of compound **4** with H_2, showing the presence of compound **5**.

4. Crystal structure determinations

Low-temperature diffraction data were collected on a D8 Quest APEX-III single crystal diffractometer with a Photon III detector and a IμS 3.0 microfocus X-ray source. Data were collected by means of ω and φ scans using monochromatic radiation λ(Mo Kα1) = 0.71073 Å. The structures were solved with SHELXT and was refined against F^2 on all data by full-matrix least squares with SHELXL.[5] All non-hydrogen atoms were refined anisotropically. Hydrogen atoms were included in the model at geometrically calculated positions and refined using a riding model, unless otherwise noted. Hydride ligands in structure **5** could not be reliably located in the difference electron density map. A summary of the fundamental crystal and refinement data are given in Table S1. Atomic coordinates, anisotropic displacement parameters and bond lengths and angles can be found in the cif files, which have been deposited in the Cambridge Crystallographic Data Centre with no. CCDC 2262392–2262394. These data can be obtained free of charge from The Cambridge Crystallographic Data Centre via www.ccdc.cam.ac.uk/data_request/cif

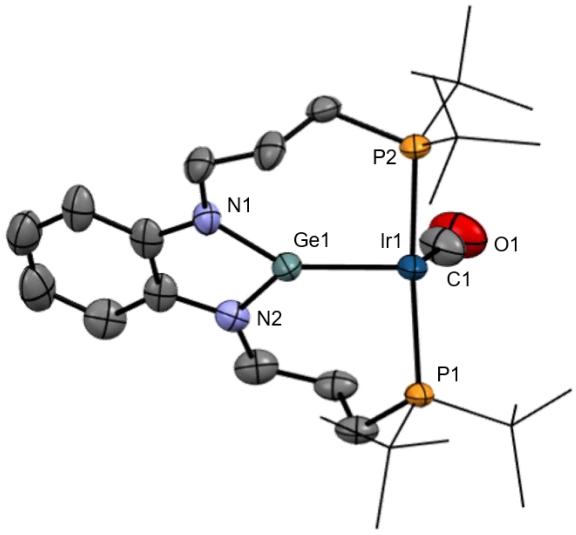

5

Figure S16. ORTEP diagram of compound **5** without the counteranion BAr^F. For the sake of clarity hydrogen atoms are excluded and tert-butyl groups have been represented in wireframe format. Hydride ligands could no be located in the difference electron density map.

Table S1. Crystal data and structure refinement for compounds **2, 3** and **4.**

	Compound **2**	Compound **3**	Compound **4**
Formula	$C_{29}H_{52}ClGeIrN_2OP_2$	$C_{61}H_{64}BF_{24}GeIrN_2OP_2$	$C_{61}H_{64}BF_{24}GeIrN_2OP_2$
Fw	806.90	1634.68	1634.68
Crystal size (mm)	0.17 × 0.12 × 0.06	0.19 × 0.07 × 0.06	0.12 × 0.11 × 0.03
Crystal system	Monoclinic	Monoclinic	Triclinic
Space group	*C*2/*c*	$P2_1/n$	*P*-1
a (Å)	17.8449 (14)	9.6734 (5)	13.3461 (6)
b (Å)	16.1593 (14)	38.7728 (17)	14.9886 (7)
c (Å)	23.0027 (18)	17.8177 (8)	16.4410 (7)
α (º)	90	90	87.795 (2)
β (º)	103.083 (5)	91.653 (2)	82.652 (2)
γ (º)	90	90	87.704 (2)
V (Å^3)	6460.9 (9)	6680.0 (5)	3257.4 (3)
T (K)	193	193	193
Z	8	4	2
ρ_{calc} (g·cm^{-3})	1.659	1.625	1.667
μ, mm^{-1} (MoKα)	5.25	2.60	2.66
F(000)	3232	3248	1624
Absorption corrections	Multi-scan	Multi-scan 0.603/0.746	Multi-scan
θ range (º)	2.1 – 26.0	2.1 – 26.0	1.9 – 25.3
Nº reflections measd	143808	106932	106971
R_{int}	0.172	0.123	0.110
Nº reflections unique	6346	13106	11779
Nº parameters/restraints	346 / 0	850 / 0	883 / 109
R_1 ($I > 2\sigma(I)$)[a]	0.042	0.054	0.053
R_1 (all data)	0.060	0.083	0.085
wR_2 (I > 2σ(I))	0.087	0.117	0.122
wR_2 (all data)	0.095	0.132	0.145
Diff. Fourier. peaks	-1.68 / 1.03	-1.32 / 1.52	-1.81 / 1.57
CCDC number	2262393	2262394	2262392

5. TON and TOF determination

Catalytic reactions were carried out on a microreactor (Man on the Moon series X102 Kit) with a total volume of 19 mL. Under a nitrogen atmosphere in the glovebox, the reactor was filled with the desired amount of base (sodium formate or NEt_3) and the corresponding catalyst precursor (0.02 mol%). The reactor was then closed and heated to the desired temperature in an oil bath. When the temperature had stabilized, 500 µL of formic acid was injected with a microsyringe.

$$H_2\ pressure\text{: } P_{H2} = \frac{P_{measured}}{2}$$

The amount of H_2 formed was calculated with the Ideal Gas Law: $n_{H2} = \frac{P_{H2}V}{RT}$

Total volume = 0.019 mL; R constant = 0.08314 bar L mol^{-1} K^{-1}

$$TON = \frac{n_{H2}}{n_{cat}}$$

$$TOF = \frac{TON}{t}$$

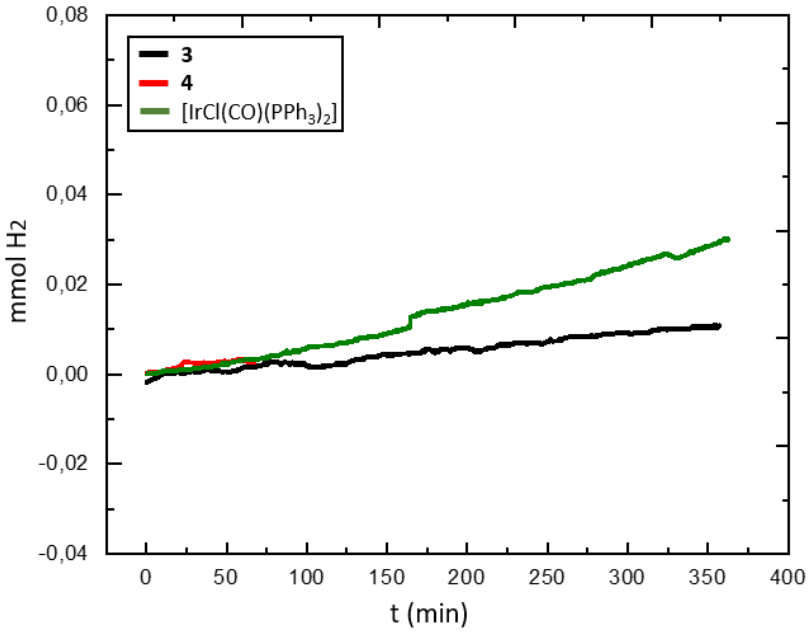

Figure S17. Generation of H_2 *vs* time for the decomposition of formic acid into H_2 and CO_2 at 173 K without additives.

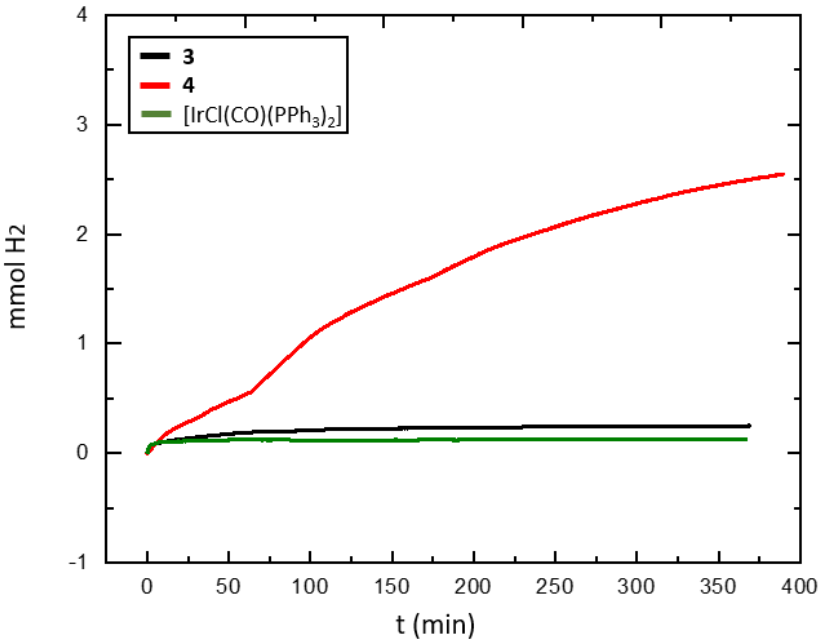

Figure S18 Generation of H_2 *vs* time for the decomposition of formic acid into H_2 and CO_2 at 263 K without additives.

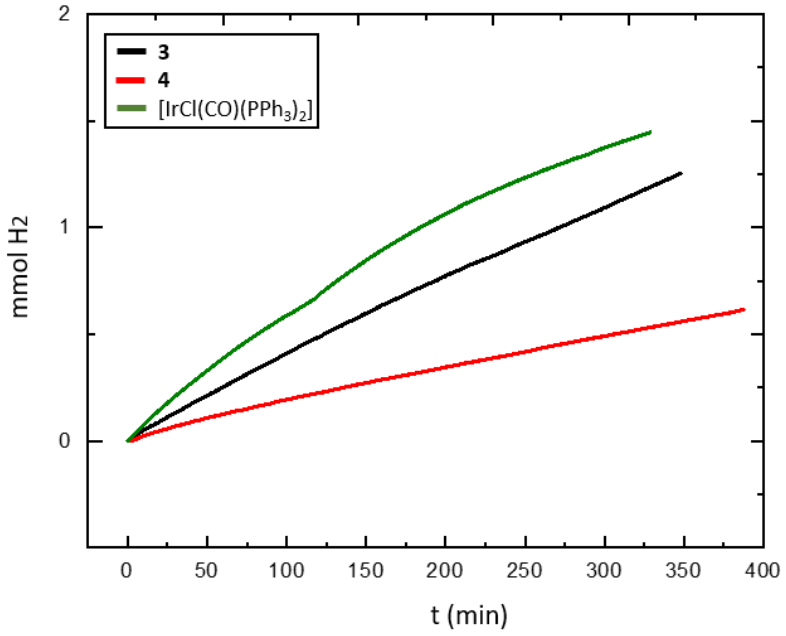

Figure S19. Generation of H_2 *vs* time for the decomposition of formic acid into H_2 and CO_2 at 263 K with Et_3N as additive.

6. Computational studies

Geometry optimization of minima and transition states was carried out with the Gaussian software package.[6] Optimizations were carried out without symmetry restrictions using DFT methods. The B3PW91 functional[7] was used with empirical dispersion taken into account by adding the D3 version of Grimme's dispersion with Becke-Johnson damping.[8] The 6-31g(d,p) basis set[9] was used for non-metal atoms and the Ir atoms were described with the SDD basis and associated electron core potential (ECP).[10] Bulk solvent effects (diethyl ether) were included during optimization with the SMD continuum model.[11] The extended wavefunction .wfx and NBO.47 files were calculated on previously optimized geometries but using the triple-ζ basis set def2-TZVP[12] basis for all atoms, which includes and ECP for Ir.[13] Wavefunction analysis and NBO analysis were performed with the Multifwn code[14] and the NBO6.0[15] software respectively. The CYLview visualization software has been used to create some of the figures.[16]

NBO analysis of the bond in 3 and 4.

Following a suggestion by an insightful referee, we inspected the natural populations of selected molecular fragments of both species **3** and **4**: the Ir—CO fragments, the NHGe fragments, comprising the PGeP ligand (**2**) but omitting the $(CH_2)_3P^tBu_2$ side arms, and the full PGeP ligand. Table S2 shows these results, which evince that not only the NBO charges of the Ge and Ir atoms undergo little changes upon chloride abstraction, but also the NBO charges of the Ir—CO fragments remain essentially the same. This therefore indicates that there is almost no change in the amount of electron density donated from the PGeP ligand to the Ir—CO fragment. In addition, the positive charge of complex **4**, resides on the PGeP ligand, being the NHGe fragment which undergoes the main change in electron population upon chloride abstraction, from ca. -0.5 electrons in the neutral species, **3**, to nearly neutral in cation **4**.

Table S2. NPA charges and Wiberg Bond Indices.

		3	*4*
NBO charges (e^-)			
atom/ molecular fragment	Ge	1.24	1.33
	Ir	-0.36	-0.42
	Cl	-0.57	-
	Ir—CO	-0.38	-0.39
	NHGe	-0.55	-0.09
	PGeP	0.95	1.39
WBO			
bond	Ge—Ir	0.43	0.46

	Ir—C(O)	1.02	0.95
	Ir—P	0.48[a]	0.47[a]
	Ge—N	0.57[a]	0.68[a]
	Ge—Cl	0.59	-

[a]Average of the two bonds.

The table below summarizes the most relevant results from the NBO analysis of **3** and **4**. In the case of **3**, six NBO are listed. The first two correspond to Lone Pairs (LP) on Ir, which are chiefly d atomic orbitals (AOs) and have low occupancies (ca. 1.7 e^-). These are delocalized onto the two π* orbitals of the CO ligand, which have occupancies of ca. 0.3 e^-. The Natural Localized Molecular Orbitals (NLMOs) associated to the above-mentioned LPs on Ir, (NLMOs are doubly occupied versions of their parent NBOs), are made up of between 7-10 % C carbonyl orbitals and less than 0.5 % Ge orbitals. This is consistent with a very low degree of back donation from Ir to Ge. The third file of the table describes two LPs, one on each nitrogen (values are averages), which are mainly p AOs perpendicular to the N-Ge-N plane. These LPs have a low degree of delocalization onto the antibonding (BD*) NBOs of the Ge-N σ linkage as deduced from the second order perturbation theory (SOPT) delocalization energies (ΔE_{ij}; the corresponding BDs are described in the 6th file). Ge is also σ-bonded to Cl (5th file) and to Ir. The latter BD is a σ bond (4th file), which has 34.2% Ir OAs and 65.8% Ge OAs contributions, consistent with the expected for a Ge → Ir dative bond.

The above description of the Ge linkage contrasts with that obtained for **4**. In this case π back bonding from Ir to the carbonyl is described in the same manner as for **3**, albeit the delocalization energies are ca. 8% smaller (7th and 8th files). The Ge—Ir bonding is described in terms of the delocalization of a LP on Ge of s^3p character (9th file), onto the Ir—C σ-BD*. This is equivalent to a Ge → Ir dative bond, but the percentage of participation of the Ge and the Ir atoms is 71.2 and 15.1 % respectively, according to the NLMO composition (compared to 65.8 and 34.2% contributions to the corresponding NBO of **3**). Importantly, the N-Ge-N linkage is described as the result of two π N—Ge BDs (13th file) and is completed by the delocalization of two sp^3 LPs (10th and 11th files), one on each nitrogen atom, onto the N-Ge-N π bonds and the lone vacancy (LV) on Ge, a non-Lewis p orbital with occupancy 0.3 e^-. As described in the main text, while π back bonding from Ir to Ge may exist, it is of little importance and the Ir—Ge interaction may be described as a single bond.

Table S3. Relevant NBO results including major donor-acceptor interactions.

NBO analysis	Entry	Donor NBO (composition) / occupancy (e^-)	Acceptor NBO / occupancy	ΔE_{ij} kcal·mol^{-1}	NLMO %parent NBO// composition %
3	1	[a]LP Ir(d) / 1.75	BD* CO (π^*_1)	38.75	87.2 // 87.2 Ir, 0.4 Ge, 2.4 O, 7.5 C
	2	[a]LP Ir(d) / 1.72	BD* CO (π^*_2)	48.77	85.7 // 85.7 Ir, 0.4 Ge, 3.4 O, 10.2 C
	3	[a]LP N(p) / [b]1.73	BD* Ge—N	4.43	86.0 // 3.9 Ge, 86.3 N
	4	[c]BD σ 0.58Ir(sd) + 0.81Ge(sp) / 1.83			
	5	[b,c]BD σ 0.39(sp3)Ge + 0.92N(sp3) / 1.92			
	6	[c]BD σ 0.41Ge(p) + 0.91Cl (sp3) / 1.95			
4	7	[a]LP Ir(d) / 1.77	BD* CO (π^*)	30.84	88.2 // 88.3 Ir, 0.5 Ge, 2.2 O, 6.8 C
	8	[a]LP Ir(d) / 1.75	BD* CO (π^*)	39.52	87.2 // 87.3 Ir, 1.0 Ge, 2.7 O, 8.3 C
	9	[a]LP Ge (s3p) / 1.44	BD* Ir—C	694.7	70.0 // 8.5 C, 15.1 Ir, 71.2 Ge
	10	[a]LP N6 (sp3) / 1.69	[d]LV Ge (p)	101.7	84.0 // 13.4 Ge, 84.0 N
	11	[a]LP N7 (sp3) / 1.69	BD* π* Ge—N	47.2	83.1 // 14.1 Ge, 83.3 N
	12	[c]BD σ 0.82C(s2p) + 0.56Ir(sd) / 1.91			
	13	[b]BD π 0.28Ge(sp7) + 0.96N(p) / 1.76			

[a]LP = Lone Pair. [b]Data are averages for the contribution of both nitrogen atoms. [c]BD = bonding (2c-2e). [d]LV = Lone Vacancy.

Table S4. AIM indicators at relevant bcps in a.u.

Complex	bond	ρ_b	G_b	V_b	H_b	$\lvert V_b \rvert / G_b$	$\nabla^2\rho$	$G_b/\rho(r_b)$	ε_b
3	Ir-CO	1.92E-01	2.32E-01	-3.61E-01	-1.29E-01	1.56E+00	4.45E-01	1.21E+00	0.010649
	Ir-Ge	7.72E-02	3.81E-02	-6.83E-02	-3.01E-02	1.79E+00	3.39E-02	4.94E-01	0.174198
4	Ir-CO	1.89E-01	2.26E-01	-3.51E-01	-1.25E-01	1.56E+00	4.36E-01	1.19E+00	0.032335
	Ir-Ge	8.36E-02	5.10E-02	-8.70E-02	-3.60E-02	1.71E+00	6.26E-02	6.09E-01	0.146223

$\boldsymbol{\rho_b}$ electron density (e·bohr^{-3}); $\mathbf{H_b}$ total energy density (hartree·bohr^{-3}); $\nabla^2\boldsymbol{\rho_b}$ Laplacian of the electron density (e·bohr^{-5}); $|\mathbf{V_b}|/\mathbf{G_b}$ ratio between the absolute electronic potential energy and kinetic energy densities; λ_i eigenvalues of the Hessian matrix; $\boldsymbol{\varepsilon_b}$ (ellipticity) ratio between the largest and smallest negative eigenvalues of the Hessian – 1.

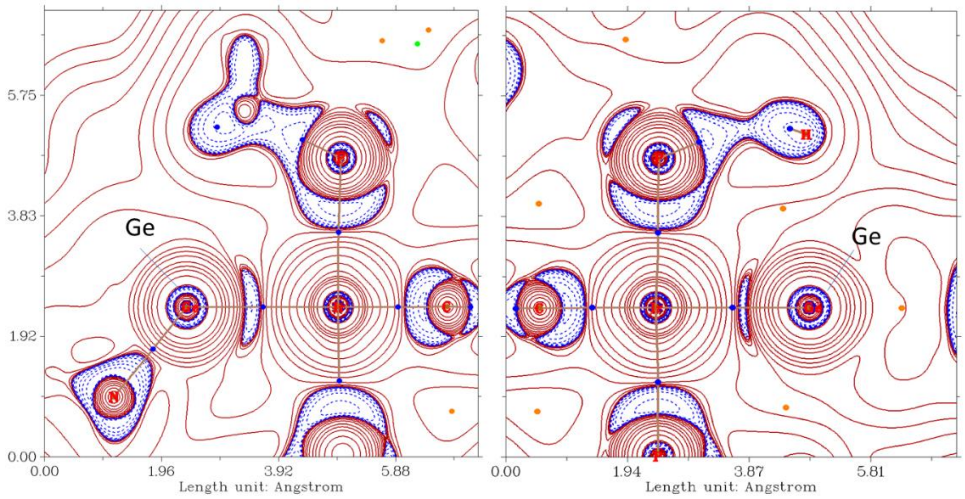

Figure S20. Critical points of the electron density of **3** and **4** and bond paths overlayed on the Laplacian of their electron density ($\nabla^2\boldsymbol{\rho}$) on the P-Ir-Ge planes. Positive and negative values of $\nabla^2\boldsymbol{\rho}$ are represented by red solid and blue dashed lines respectively.

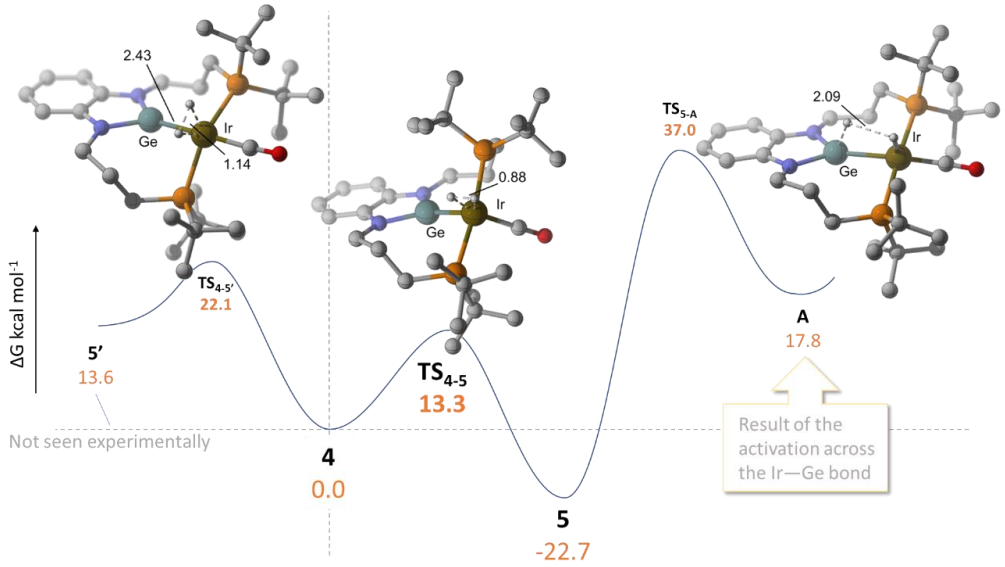

Figure S21. Calculated energy profile (G) for the activation of dihydrogen at **4** and optimized geometry for the transition states.

7. References

1. L. Vaska, J. W. DiLuzio, *J. Am. Chem. Soc.*, 1961, **83**, 2784.
2. (a) E. H. Kwan, H. Ogawa, M. Yamashita, *ChemCatChem* 2017, **9**, 2457-2462; (b) S. Morisako, S. Watanabe, S. Ikemoto, S. Muratsugu, M. Tada, M. Yamashita, *Angew. Chem. Int. Ed.* 2019, **58**, 15031-15035.
3. (a) D. H. Harris, M. F. Lappert, *J. Chem. Soc., Chem. Commun*. 1974, 895; (b) M. J. S. Gyanane, D. H. Harris, M. F. Lappert, P. P. Power, P. Riviere-Baudet, *J. Chem. Soc., Dalton Trans.* 1977, 2004.
4. N. A. Yakelis, R. G. Bergman, *Organometallics* 2005, **24**, 3579-3581.
5. G. M. Sheldrick, *Acta Cryst.* 2008, **A64**, 112.
6. Gaussian 09, Revisions E.01 and B.01, M. J. Frisch, G. W. Trucks, H. B. Schlegel, G. E. Scuseria, M. A. Robb, J. R. Cheeseman, G. Scalmani, V. Barone, B. Mennucci, G. A. Petersson, H. Nakatsuji, M. Caricato, X. Li, H. P. Hratchian, A. F. Izmaylov, J. Bloino, G. Zheng, J. L. Sonnenberg, M. Hada, M. Ehara, K. Toyota, R. Fukuda, J. Hasegawa, M. Ishida, T. Nakajima, Y. Honda, O. Kitao, H. Nakai, T. Vreven, J. A. Montgomery, Jr., J. E. Peralta, F. Ogliaro, M. Bearpark, J. J. Heyd, E. Brothers, K. N. Kudin, V. N. Staroverov, T. Keith, R. Kobayashi, J. Normand, K. Raghavachari, A. Rendell, J. C. Burant, S. S. Iyengar, J. Tomasi, M. Cossi, N. Rega, J. M. Millam, M. Klene, J. E. Knox, J. B. Cross, V. Bakken, C. Adamo, J. Jaramillo, R. Gomperts, R. E. Stratmann, O. Yazyev, A. J. Austin, R. Cammi, C. Pomelli, J. W. Ochterski, R. L. Martin, K. Morokuma, V. G. Zakrzewski, G. A. Voth, P. Salvador, J. J. Dannenberg, S. Dapprich, A. D. Daniels, O. Farkas, J. B. Foresman, J. V. Ortiz, J. Cioslowski, and D. J. Fox, Gaussian, Inc., Wallingford CT, 2010.
7. J. P. Perdew, in *Electronic Structure of Solids '91*, Ed. P. Ziesche and H. Eschrig (Akademie Verlag, Berlin, 1991, **11**.
8. S. Grimme, S. Ehrlich and L. Goerigk, *J. Comp. Chem*. 2011, **32**, 1456-65. DOI: 10.1002/jcc.21759
9. (a) R. Ditchfield, W. J. Hehre, J. A. Pople, *J. Chem. Phys.* 1971, **54**, 724–728; (b) W. J. Hehre, R. Ditchfield, J. A. Pople, *J. Chem. Phys*. 1972, **56**, 2257–2261; (c) P. C. Hariharan, J. A. Pople, *Theor. Chim. Acta* 1973, **28**, 213–222; (d) M. M. Francl, W. J. Pietro, W. J. Hehre, J. S. Binkley, M. S. Gordon, D. J. DeFrees, J. A. Pople, *J. Chem. Phys*. 1982, **77**, 3654–3665.
10. D. Andrae, U. Haeussermann, M. Dolg, H. Stoll, H. Preuss, *Theor. Chim. Acta* 1990, **77**, 123–141.

11. A. V. Marenich, C. J. Cramer, D. G. Truhlar, *J. Phys. Chem. B* 2009, **113**, 6378–6396.
12. F. Weigend, R. Ahlrichs, *Phys. Chem. Chem. Phys*., 2005, **7**, 3297-305. DOI: 10.1039/B508541A
13. D. Andrae, U. Häußermann, M. Dolg,H. Stoll, H. Preuß, *Theor. Chim. Acta* 1990, **77**, 123-141. DOI: 10.1007/BF01114537
14. (a) Multiwfn, v. 6.0. http://sobereva.com/multiwfn/ (b) T. Lu, F. Chen, *J. Comput. Chem*. 2012, **33**, 580-592.
15. E. D. Glendening, C. R. Landis, F. Weinhold, *J. Comput. Chem*. 2013, **34**, 1429-1437; (b) E. D. Glendening, J. K. Badenhoop, A. E. Reed, J. E. Carpenter, J. A. Bohmann, C. M. Morales, C. R. Landis, F. Weinhold, "NBO 6.0." Theoretical Chemistry Institute, University of Wisconsin: Madison, 2013. Available at: https://chem.wisc.edu/
16. CYLview, 1.0b; C. Y. Legault, Université de Sherbrooke, **2009** (http://www.cylview.org/).